THE JOURNAL OF PHYSICAL CHEMISTRY B

pubs.acs.org/JPCB Article

Blind Resolution of Lifetime Components in Individual Pixels of Fluorescence Lifetime Images Using the Phasor Approach

Alexander Vallmitjana,[§] Belén Torrado,[§] Alexander Dvornikov, Suman Ranjit,* and Enrico Gratton*

Cite This: *J. Phys. Chem. B* 2020, 124, 10126–10137 Read Online

ACCESS | Metrics & More | Article Recommendations | Supporting Information

ABSTRACT: The phasor approach is used in fluorescence lifetime imaging microscopy for several purposes, notably to calculate the metabolic index of single cells and tissues. An important feature of the phasor approach is that it is a fit-free method allowing immediate and easy to interpret analysis of images. In a recent paper, we showed that three or four intensity fractions of exponential components can be resolved in each pixel of an image by the phasor approach using simple algebra, provided the component phasors are known. This method only makes use of the rule of linear combination of phasors rather than fits. Without prior knowledge of the components and their single exponential decay times, resolution of components and fractions is much more challenging. Blind decomposition has been carried out only for cuvette experiments wherein the statistics in terms of the number of photons collected is very good. In this paper, we show that using the phasor approach and measurements of the decay at phasor harmonics 2 and 3, available using modern electronics, we could resolve the decay in each pixel of an image in live cells or mice liver tissues with two or more exponential components without prior knowledge of the values of the components. In this paper, blind decomposition is achieved using a graphical method for two components and a minimization method for three components. This specific use of the phasor approach to resolve multicomponents in a pixel enables applications where multiplexing species with different lifetimes and potentially different spectra can provide a different type of super-resolved image content.

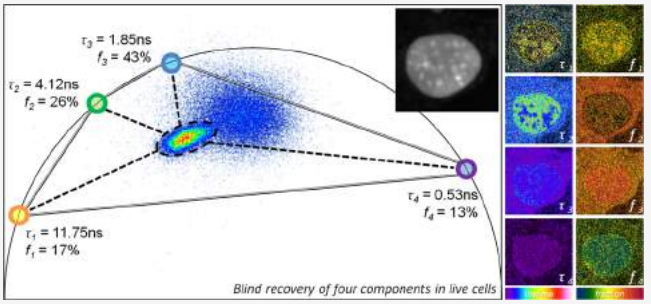

INTRODUCTION

Resolving multiple decay components in the same pixel is a very different task than resolving different components spatially separated in different parts of the fluorescence lifetime imaging microscopy (FLIM) image.[1−3] The phasor approach has become popular because of its ease of use and also for being fit-free and therefore not affected by artifacts introduced during the fit.[1,4−9] For example, in the case of NAD(P)H, the form bound to an enzyme and the free form of NAD(P)H, with good approximation, decay as single exponentials, although the free form is composed of several species decaying with slightly different lifetimes.[10−12] Because the law of linear phasor combination[3,13] holds for multiple components, an experimental pixel that has the two components of nicotinamide adenine dinucleotide (reduced) (NADH) (bound and free) will fall in the line joining the position of the two pure species (bound and free,[14] although they could be decaying as multiexponentials).[3,14,15] This property has been exploited by measuring the position of the pixel along that line using a graphical approach.[16,17] In practice, we resolve the decay at each pixel along the line in the two species (bound and free NAD(P)H) and their relative fractional intensities.[3,14] The issue becomes more complicated when the combinations of three or more components exist within a pixel. When the components are two or three, this problem can be solved graphically, and here, we describe these algorithms. The graphical approach was published earlier.[17,18] The graphical decomposition is simple if we know the location in the phasor plot of the pure species. In such a case, the fractional intensity contributions of three species can be obtained using the rules of linear algebra.[17,18] However, when the lifetimes of the pure species are not known in advance, the problem of resolving the unknown lifetimes becomes difficult under the typical FLIM conditions in which only about 100 photons are collected at each pixel of an image. Global fitting methods (spatially averaging) have been used,[19−22] but so far, we do not have a pixel-wise "blind" method to resolve components and their intensity fractions, that is, the relative abundance of the species, which is the subject of this manuscript. The term *blind* refers to the fact that we do not have any *a priori* knowledge of either the fractions or the lifetimes of the components contributing to the lifetime curve at a particular pixel.

Received: July 29, 2020
Revised: October 21, 2020
Published: November 3, 2020

https://dx.doi.org/10.1021/acs.jpcb.0c06946
J. Phys. Chem. B 2020, 124, 10126−10137

In the Supporting Information of this paper, we briefly introduce the definition of the phasor transform and the representation of the decay curve as a point in the phasor plot, the concept of the harmonic content of the data at each pixel of the image, and the specific processing pipeline used in this work.

To establish some general principles, because a pixel on the phasor plot is identified by two coordinates (g and s, as shown in the Supporting Information), this gives us two constraints, so, at most, we can solve a system with two unknowns. However, if we calculate the phasor transform of our data into higher harmonics of the original frequency of acquisition and the data do carry additional information in the harmonic content, then additional unknowns can be determined. In general, the measurement of multiple harmonics is not always possible because it depends on the specific electronic characteristics of the lifetime device being used to measure the decay. The field programmable gate array (FPGA)-based device used here carries information up to the seventh harmonic. Supposing the measurement device does have the capability of capturing higher harmonics, one can then obtain these harmonics by computing the phasor transform of the required order (see the Supporting Information for more details). For example, if we have the first and second phasor harmonics, in principle, we can find four unknowns. In such an example, it would be possible to calculate two lifetimes and one relative intensity fraction. If we have three harmonics in the phasor plot, we have a total of six parameters (two coordinates per harmonic) and we can obtain three lifetimes and three intensity fractions. In principle, this operation could be carried out if the decays were to be measured in the time domain, but the lack of sufficient statistics in terms of total photons collected in a pixel and the need to account for the instrument response function have prevented the resolution of more than two components in the same pixel in FLIM images.

The blind analysis of components in each pixel will allow us to obtain the relative abundance of multiple species in every pixel of an image from a single measurement—using spectral[23,24] and lifetime information. With the technique described in this manuscript available, experiments which require the measurement of many components in the same pixel, for example, for biomedical diagnostic applications, gene expression, and other fundamental applications in biology, can be performed.

In this paper, first, we describe the graphical and analytical algorithms employed. Next, we simulate various combinations of components with and without noise added to the lifetime components and to the phasor coordinates g and s of the harmonics to test the algorithm. Then, we use a mixture of two to four single exponential dyes in solutions, and finally, to further test the method, we show images of biological samples. We show an example with live cells stained with nuclear dyes and another example in which we measured autofluorescence from mice liver tissue samples [fed with normal diet and high fat and high cholesterol diet called Western diet (WD)]. In both biological examples, we have at least three components in some pixels to demonstrate the applicability of the blind decomposition algorithm.

DEFINING THE PROBLEM

The Supporting Information of this manuscript contains detailed information about the definition of the phasor approach and its graphical interpretation. Based on the properties of vector addition in phasor plots (also called the linear combination of the phasor), the starting point is the constraint that the data point in the phasor representation must be a weighted sum of the N coordinates of the pure component species that are contributing to the fluorescence in this pixel[1,3,5,7]

$$\sum_{1}^{N} f_i g_i = G \tag{1}$$

$$\sum_{1}^{N} f_i s_i = S \tag{2}$$

$$\sum_{1}^{N} f_i = 1 \tag{3}$$

Here, the measured data point is at the coordinates (G, S) which are expressed as the sum of N components, with coordinates (g_i, s_i), each with its corresponding fractions f_i. The geometrical interpretation of the constraints of eqs 1 and 2 is that a data point is located at the weighted barycenter of the polygon, the vertices of which are the positions of the pure components. The sum of the fractions is unity by construction.

Additionally, because of the fact that the pure components are, by definition, single exponential decays, we add the constraint that they have to lie on what, in the phasor representation, is known as the universal semicircle. This is the relation between the coordinates; $s_i^2 = g_i - g_i^2$, being the equation of the universal circle. The other consideration that also only holds on the universal circle is that because of the properties of the phasor transform, for a pure mono-exponential components component, we can relate the coordinates of any harmonics of the same lifetime (see the Supporting Information and Figures 1 and 2).

Finally, the key point is that if the decay data are acquired in a way that their higher harmonics can be obtained, then eqs 1 and 2 can be written for each of the harmonics where in each of these pairs of equations, the fractions f_i are consistent between eqs 1 and 2 (see the Supporting Information). At this point, we are left with a set of n pairs of equations, one for each harmonic, and the relationship between the fractions (eq 3). Using the equation of the universal circle, we can express all the s_i coordinates of the pure mono-exponential components in terms of the g_i coordinate which depends on the lifetime, at the cost of adding nonlinearity to the system. Similarly, using the relation between the coordinates on the universal circle and its harmonics, we can express all the higher harmonics in terms of the first one. Finally, we can always use (eq 3) to express one of the fractions in terms of the other $N - 1$.

For the general case of N components, we are left with a total of $(2N - 1)$ unknowns, the g_i and s_i coordinates for the N components and $N - 1$ of the weights f_i. This means that in order for the problem to be solvable, we need to measure at least N harmonics to write down the $2N$ nonlinear equations. The harmonics must be measured at each pixel of the image, which is doable with modern FLIM acquisition electronics.[25]

METHODS

Resolving Two Components Using a Graphical Approach. The system of equations defined in the Introduction can be solved, for example, by least squares methods for every possible combination of lifetimes or using

https://dx.doi.org/10.1021/acs.jpcb.0c06946
J. Phys. Chem. B 2020, 124, 10126−10137

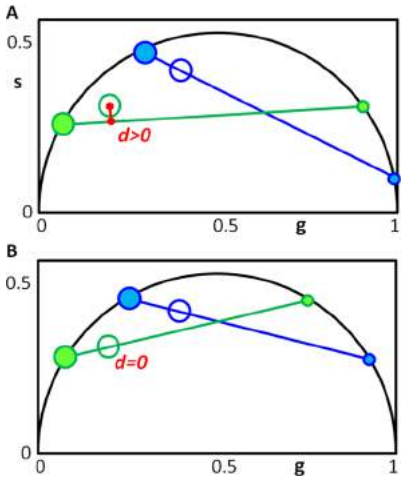

Figure 1. Graphically finding two unknown lifetime components and their relative fractional intensities. (A) Universal circle is scanned for candidate components. For each position of the first component (small blue dot), a line is drawn through the data point (blue empty circle) and the second point is found where the blue line meets the universal circle (large blue filled circle). The second harmonic ($h2$) for the candidate components are obtained mathematically: small green dot and the large green filled circle. A line is drawn through them (green line). (B) Solution is the only lifetime pair that has the lines (blue and green) going through the data points for the two harmonics, that is, when the distance from the green line to the green empty circle is zero. The relative fractions are obtained by the ratios between the distances from the filled dots to the empty circles in both sides of the line.

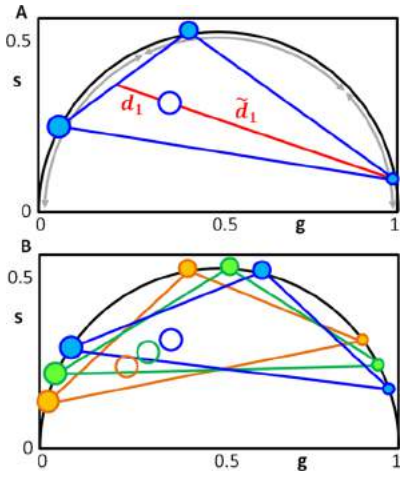

Figure 2. Finding the three lifetime components in the universal circle. (A) Schematic configuration of three components generating a data point (ring in the middle). As an example, the ratio between the two distances is related to the intensity fraction of the component located in the short lifetime region; $f_1 = d_1/(d_1 + \tilde{d}_1)$. In the same manner, the other two fractions can be obtained for the other two components. (B) Solution to the three-component problem is the only combination of components such that the three fractions are the same in each of the triangles composed of the three harmonics (blue–green–orange). The short, medium, and long lifetime components in each harmonics are depicted by increasingly larger filled circles.

minimization techniques such as the simplex algorithm or gradient-based algorithms. However, we found that for the case of two components, a geometric graphical algorithm is much faster and, more importantly, does not require an initial guess, as is the case for the minimization algorithms. For the purpose of this work, we use the graphical method to illustrate the role of the harmonics and the principle we are using to determine the parameters of a blind system using the constraints that are given by the requirement that the experimentally determined harmonics impose on the possible locations of the unknown lifetimes and their fractional intensities.

In the case of two components, the experimental data at each pixel are the first ($h1$) and second ($h2$) harmonic coordinates from the FLIM measurement of a system that contains two exponential components, as shown in Figure 1 (the data are the blue and the green empty circles inside the universal semicircle).[26] The algorithm consists in finding the pure mono-exponential lifetimes and the fractional components that have generated the data (the empty circles) for both harmonics (blue and green).

Starting with a point on the universal circle (the small blue dot at the right, Figure 1A), we trace a line from this point passing through the experimental data point (blue empty circle, Figure 1A). This line intersects the universal circle at a point which determines the second lifetime (large filled blue dot on the universal circle). The distance between the blue line and the experimental point is zero by construction (Figure 1A). We scan the universal circle, and for each position of the candidate components (again, blue filled circles), we calculate the corresponding second harmonic positions of the two candidate lifetimes (green filled circles). In general, the line joining these second harmonics of the candidate lifetimes will not pass through the second harmonic of the data point (empty green ring). We keep repeating this process for all possible positions of the candidate until the distance in the second harmonic is minimal. This is the solution for two components. For the fractional intensities, we find the relative distances of the two line segments on either side of the data point (in either of the harmonics). The specific solution is shown in Figure 1B.

Resolving *N* Components. Before moving into the general case, we developed a similar graphical approach for resolving three components by the graphical method. Again, we scan the phasor plot semicircle for all possible combinations of the three components with the addition, as reasoned in the Introduction that we now need three harmonics at each pixel. For each of the possible combinations of three candidate components, the fractions that would generate the data in each of the three harmonics are calculated and the solution is the one combination of components that satisfies that the fractions are the same.

Figure 2 shows the approach for three arbitrary components. Similar to the previous case, the algorithm scans the three-dimensional space defined by the three components and finds the combination of them that generates the data points in the three harmonics with the same intensity fractions.

The set of equations (eq 1), (eq 2), and (eq 3) allows us to analytically express the three fractions in terms of the coordinates. From (eq 3) $f_3 = 1 - f_2 - f_1$ and additionally for the other two fractions

$$f_1 = \frac{(G - g_3)(s_2 - s_3) - (g_2 - g_3)(S - s_3)}{(g_1 - g_3)(s_2 - s_3) - (g_2 - g_3)(s_1 - s_3)} \quad (4)$$

$$f_2 = \frac{(G - g_3)(s_1 - s_3) - (g_1 - g_3)(S - s_3)}{(g_2 - g_3)(s_1 - s_3) - (g_1 - g_3)(s_2 - s_3)} \quad (5)$$

https://dx.doi.org/10.1021/acs.jpcb.0c06946
J. Phys. Chem. B 2020, 124, 10126–10137

This allows obtaining the fractions for each combination of candidate lifetimes for each harmonic and finding the lifetime combination in which the fractions are the same (with some tolerance). One does not really need to scan the whole space of possibilities and can exclude the permutations of components. Additionally, one does not need to cover the cases in which the three components form a triangle with the data point (the harmonics) outside of it (corresponding to negative fractions and/or fractions above unity).

Figure 2 follows the same color and symbol code used in Figure 1; the experimental points are indicated with empty circles, and individual components are indicated by filled circles (blue, green, and orange represent the first, second, and third, respectively).

This graphical algorithm is computationally simple. Three nested loops are present for the three independent lifetimes, one inside the other, for each iteration solving expressions in eqs 4 and 5. The number of steps in which the circle is divided determines the computational search time. This is the reason why the algorithm cannot realistically be upgraded to a higher number of components; the computational time scales with the *N*th power of the number of steps in each lifetime component.

Our alternative to the graphical search approach is a minimization-based approach. This approach allows the possibility of writing a general algorithm to the problem to *N* components, at the cost of the possibility of falling in a local minimum. The function to be minimized can be constructed from equations (eqs 1 and 2) written for three harmonics. One can define a distance function as the sum of the squared differences of each of the terms on either side of the equality. The mathematical formulation is detailed in the Supporting Information.

In our website, we provide the SimFCS program with the instructions to perform simulations on the effect of combining two, three, or four components and using harmonics to resolve the mixture and to perform the general blind component analysis, given a set of FLIM measurements (https://www.lfd.uci.edu/).

Experimental System and Data Acquisition. Data acquisition and analysis were performed using the Globals for Images-SimFCS software (available for free download at https://www.lfd.uci.edu/). The deep imaging *via* emission recovery (DIVER) microscope (described in refs 27, 28) was used for imaging. This multiphoton microscope utilizes a tunable pulsed InSight DS+ laser (Spectra-Physics, Santa Clara, USA), operating at an 80 MHz repetition rate. Dye solutions and nuclear stains were excited using the Olympus LUMPlanFL 40×/0.80NA W objective, following a two-photon excitation scheme at 800 nm and an average laser power of 5−10 mW at the sample, and were collected using the DIVER detector that does not require an objective for collection of fluorescence. Images of 256 × 256 pixels were acquired at 32 μs/pixel dwell time and averaged for 10 frames/image. Liver samples were excited at 740 nm, and the signal was collected using a 400−500 nm filter; tiling was performed using a 10×/0.1NA air objective. The microscope is connected to a 320 Fast-FLIMbox (ISS, Inc., Champaign-Illinois, USA) to allow FLIM measurements and phasor analysis.[29] The FLIMbox utilizes Spartan 6 FPGA and allows multifrequency data analysis up to the seventh harmonic with a fundamental frequency of 80 MHz.[25] We would like to note that other commercial microscopes with similar FLIM capabilities can be used as well for equivalent data acquisition and processing, such as the Leica Falcon or instruments that use time domain devices by PicoQuant. The only requirement is that the setup is carried out correctly to access the higher harmonic information, that is, the repetition frequency is long enough to capture the whole decay.

Preparation of Dye Mixtures. The following dyes with the known fluorescence lifetimes were used as individual components and in mixtures: 5-dimethylaminonaphthalene-1-sulfonic acid (dansyl acid) (TCI America, Portland, OR), fluorescein (Sigma-Aldrich, St. Louis, MO), eosin Y (Sigma-Aldrich, St. Louis, MO), and sulfo-cyanine3 carboxylic acid (sulfo-Cy3) (Lumiprobe, Hunt Valley, Maryland). Solutions were prepared by dissolving the solid in phosphate buffer pH 7.4 and diluting them to the proper concentration (∼10−20 μM) to yield approximately the same signal level. The individual dye solutions were then mixed together, and these mixtures were imaged using the DIVER microscope. When measuring the pure components (not mixed), the dyes display a phasor value close to the universal semicircle under our experimental conditions. The fluorescence lifetimes were measured to be 11.8, 4.1, 1.1, and 0.2 ns for dansyl acid, fluorescein, eosin Y, and sulfo-Cy3 solutions, respectively, and these values match very well with published data.[30−33]

Cell Culture and Staining with Nuclear Probes. NIH3T3 (ATCC, Manassas, VA) cells were cultured in Dulbecco's modified Eagle medium (DMEM, Thermo Fisher Scientific, Waltham, MA) supplemented with 10% fetal bovine serum (FBS, Sigma-Aldrich, St. Louis, MO), streptomycin (100 μg/mL), and penicillin (100 U/mL) at 37 °C in a 5% CO_2 incubator. Cells were plated in fibronectin (Sigma-Aldrich, St. Louis, MO)-covered glass bottom dishes (Mattek, Ashland, MA) 24 h prior to FLIM imaging. We permeabilized live cells with 0.1% Triton X-100 for 10 min at 4 °C, to improve dye staining,[34] and washed them twice (before and after the treatment) with 1× Dulbecco's phosphate buffer solution (DPBS). Multiple staining of the cells was performed sequentially, as described previously.[18] The dyes used in the cells are different dyes than the ones used in the solution mixture. First, cells were incubated with rose bengal (10 μg/mL, Sigma-Aldrich, St. Louis, MO) for 5 min at 37 °C and washed twice with DPBS. After that, cells were incubated for at least 5 min with the NucBlue Live ReadyProbes reagent (working solution was a dilution 1/30 of the manufacturer's recommendation of 1 drop/1.5 mL, Thermo Fisher Scientific, Waltham, MA) and acridine orange (13 ng/mL, Sigma-Aldrich, St. Louis, MO). Dilutions of each dye were adjusted individually to obtain a similar amount of photons in all of them, and they were prepared in a DMEM phenol-free, high glucose, HEPES medium (Thermo Fisher Scientific, Waltham, MA).

Liver Tissue Samples. Male C57BL/6J mice were purchased from Jackson Laboratories (Bar Harbor, ME) and fed with 42% milkfat, 34% sucrose, and 0.2% cholesterol, Harlan Teklad, TD.88137 WD, or matched 10% fat, Harlan Teklad TD.08485 LF. We imaged flash frozen liver slices (5 μm thick), embedded in OCT and obtained from mice that were fed with a low-fat (LF) diet or high-fat high-cholesterol WD.[35]

RESULTS

Simulations. The two-component graphical algorithm described in the previous section was implemented in MATLAB and is also implemented in SimFCS software

https://dx.doi.org/10.1021/acs.jpcb.0c06946
J. Phys. Chem. B 2020, 124, 10126−10137

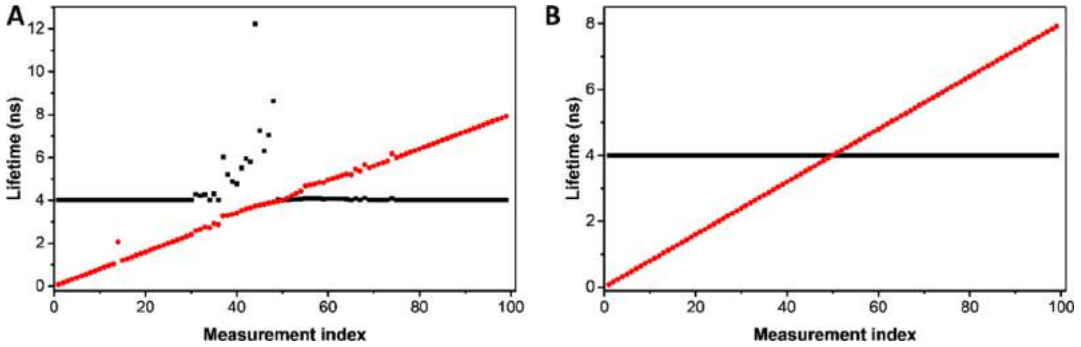

Figure 3. Simulations for two components, one fixed and one variable. The points in the graphs are the recovered lifetimes. (A) Lifetime component of 4 ns (black) (right) is mixed in the same pixel in equal fractional intensity with a variable lifetime component (red) that spans the range from 0 to 8 ns. When the two lifetime components become similar (simulation measurements from 40 to 50), the algorithm shows a lifetime component at around 4 ns and another component whose value and fraction are undefined, as it should because in this range, there is effectively only one lifetime. (B) We fixed the fractional intensity of the first component to have the same value for all the simulations. In this case, the two lifetime values are recovered perfectly even if they are very close to one another.

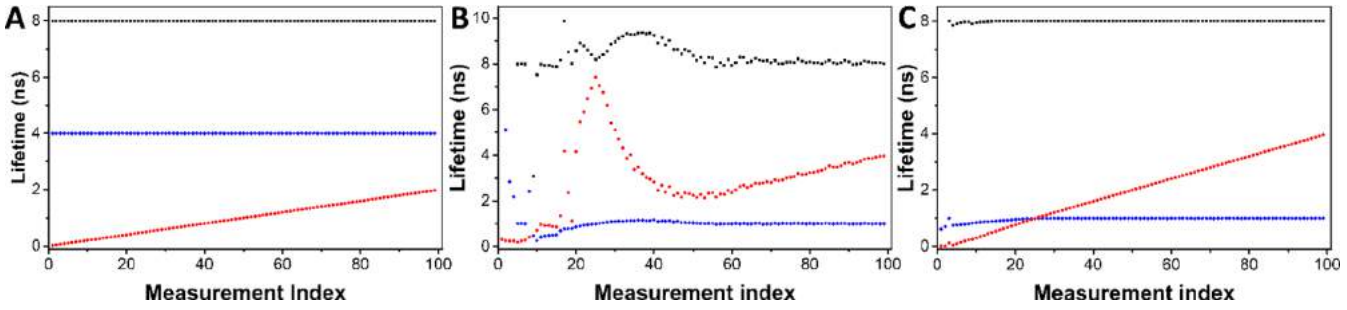

Figure 4. Simulation for blind recovery of three components and three intensity fractions. The points in the graphs are the recovered components. (A) One lifetime component simulated was 8 ns (black), another was 4 ns (blue), and a third lifetime component was added with variable lifetime (red) from 0.02 to 2.0 ns in steps of 0.02 ns. The fractional intensities were 0.5, 0.3, and 0.2 for the three components, respectively. Panel A shows that this system can be recovered exactly in the simulations because the lifetimes are different in all the ranges of the simulation. (B) Recovery of the three components when two lifetimes become very close. The lifetime set was 8 ns (black), 1 ns (blue), and a variable lifetime from 0.02 to 4 ns (red). As this variable component lifetime increases, the recovered value of the 8 ns component changes from around 8 ns, reaching a maximum of about 9 ns when the variable component is similar to the second components at 1 ns. As the variable component continues to increase in lifetime value, it causes a decrease in long lifetime returning to 8 ns and a stabilization of the 1 ns component when the added component reaches a value of 2 ns or longer. This simulation shows that the blind independent determination of three components is difficult because one component can influence the others when two of the components have similar lifetimes. (C) However, if we fix the relative contribution of the long components to the value of 0.5, we obtain a perfect recovery of the three lifetimes. This simulation demonstrates that the lifetimes and fractions are correlated. If we fix the fraction of one component, then the systems can be recovered exactly.

(available at https://www.lfd.uci.edu/) and is very fast, about 0.5 s to resolve an image of 256 × 256 points into two components and their intensity fractions. Because the algorithm explores the entire universal semicircle in 720 points, we can guarantee that even if there are local minima, we converge to the absolute minimum. If the components are very close in lifetime (within 0.5 ns), the algorithm tends to be more sensitive to noise and to return a value that is in the middle of the two real components, as shown in Figure 3, that is, the solution is close to a case with only one true component.

For both the two- and the equivalent three-component graphical methods, the computational time of the algorithms depends on the number of steps one divides the universal circle, which in our implementation, for steps of 0.125°, it finds the solution in about 0.5 ms per point, which means about 30 s for an image of 256 × 256 pixels. However, by decreasing the size of the step, we always find the same solution but using more computational time. By exploring the entire phasor semicircle, we ensure that all possible lifetimes are explored and avoid falling in a local minimum. However, for three components, we found that the minimum of the distance function is not well defined unless the lifetimes are well separated, as shown in Figure 4.

The squared sum of differences of the terms on either side of the equality symbol in eqs 1 and 2, defines an N dimensional surface as a function of the N components. The solution to our problem is the (one) zero on this surface. Even if such a minimum is found in a relatively flat region of the surface, the results of the algorithm are exactly reproducible, although the values may not be accurate, as shown in Figure 4B. The reproducibility is due to the path followed by the search algorithm, which always explores the same surface following the same trajectory.

We note that the principle of exploring the universal semicircle can be used for four or more components, but the flatness of the aforementioned surface can become a formidable obstacle for finding the solutions without any prior knowledge of the parameters.

Our final implementation, generalizable to N components, uses a computational minimization method[36−38] that is relatively fast depending on the parameters, in the order of 1 ms per pixel. The computational method is based on nonlinear

https://dx.doi.org/10.1021/acs.jpcb.0c06946
J. Phys. Chem. B 2020, 124, 10126−10137

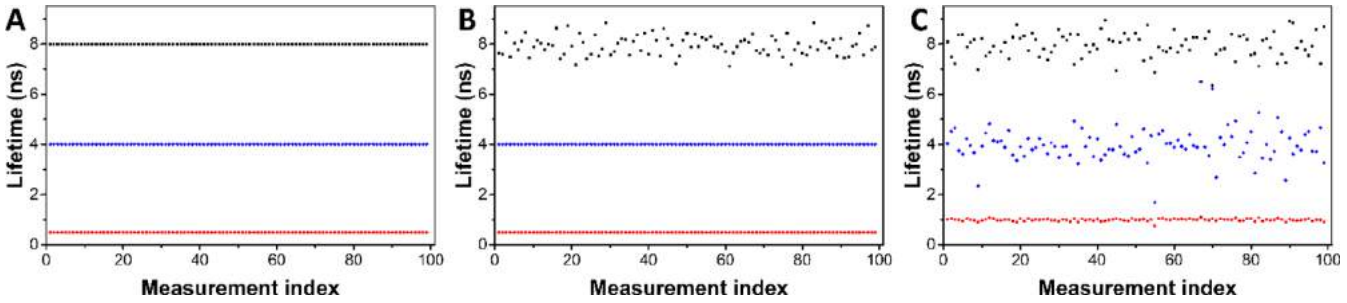

Figure 5. Effect of noise on the recovery of components. The points in the graph are the recovered lifetimes. (A) Simulation of three lifetime components, no noise added. Black, blue, and red represent 8, 4, and 1 ns lifetimes in each individual measurement/simulation. (B) Noise is added only to the 8 ns component. Note that the other component lifetimes are not affected by the noise added to the 8 ns component. (C) Noise is added to the harmonics (not lifetime) of the 8 ns component. Here, we show that other components (4 ns/1 ns) get affected when the noise is added to the harmonics.

minimization with an initial application of the Levenberg–Marquardt algorithm followed by the simplex methods, and this sequence is repeated three times. The computational method is easily extended to four or five components, but some issues regarding the effect of added noise need to be considered. In Figure 4, we simulated two lifetimes of different ranges showing that they influence each other, when they are similar in value, but we have not added noise to the lifetime or intensity values. In Figure 4, we also show the effect of having two of the lifetimes of a similar value. As an example, we show the effect of fixing the value of the fractional intensity contribution of one lifetime component in panel C, and we further describe and implement fixing the lifetime value using real data from solutions in the following section.

We used simulations to test the recovery algorithm with added noise in the lifetime values and intensity fractions, as shown in Figure 5. In this set of simulations, we sampled measurements of three Gaussian lifetime distributions centered on 8, 4, and 0.5 ns with a standard deviation of 0.5 ns to the 8 ns component. When noise is added to one of the components, the noise does not propagate to the other components or fractions, as seen in Figure 5B, although, as expected, it does broaden the distribution of recovered values of the long component, while keeping the mean values the same.

There is a fundamental difference in the simulations if noise is applied to the lifetime components and their fractional intensities and then propagated to the harmonics compared to the other possibility in which noise is added to the harmonic coordinates after phasor transform. In the first case (noise added to the lifetime), the noise in one component has no effect on the values obtained for the other components. This is shown in Figure 5B where the recovered component has the noise we added but the other components have no noise. This happens because in the phasor representation, each component is orthogonal to the others and the noise does not propagate to the other components. In the second scenario, when noise is added to the harmonics which are combinations of lifetime and fractions (eqs 1 and 2), the recovered components are all affected by the added noise in a correlated way (Figure 5C) because of the linear relationships of the harmonics to the lifetime components and fractional intensities in eqs 1 and 2. This different behavior is important because the harmonic method proposed in this paper ultimately depends on the noise in the harmonics (the data) which affects all values of the recovered lifetimes and fractional intensities (Figure 5C). Tables 1–3 show this effect numerically. For this reason, we tested the method with the hardest possible situation by adding independent random noise to each harmonic, which, in general, will not be the case.

Table 1. Gaussian Noise is Only Applied to the Lifetime Distribution of the First Component (10 ns).[a]

	recovered		
simulated	no noise	0.05 G-noise	0.10 G-noise
10.0	10.0 ± 0.001	10.0 ± 0.047	10.0 ± 0.100
4.0	4.0 ± 0.001	4.0 ± 0.001	4.0 ± 0.001
0.5	0.5 ± 0.001	0.5 ± 0.001	0.5 ± 0.001

[a]All values are in ns, and recovered data are shown as mean ± standard deviation (std).

Table 2. Gaussian Noise is Applied to Phasor Coordinates of Harmonics of Component 1 (and Instead of Lifetime before Phasor Transform).[a]

	recovered		
simulated	no noise	0.001 G-noise	0.004 G-noise
10.0	10.0 ± 0.001	9.57 ± 0.05	9.50 ± 1.68
4.0	4.0 ± 0.001	4.07 ± 0.38	4.70 ± 1.61
0.5	0.5 ± 0.001	0.50 ± 0.03	0.49 ± 0.14

[a]The components are recovered using the harmonics. Notice that Gaussian noise added is smaller than Tables 1 and 3. All values are in ns, and recovered data are shown as mean ± std.

Table 3. Gaussian Noise is Applied Only to Harmonics of Component 1 but the Fractions are Fixed to Their Known Values[a]

	recovered		
simulated	no noise	0.05 G-noise	0.10 G-noise
10.0	10.0 ± 0.001	10.02 ± 0.28	10.06 ± 1.29
4.0	4.0 ± 0.001	3.99 ± 0.09	4.11 ± 0.57
0.5	0.5 ± 0.001	0.50 ± 0.01	0.50 ± 0.05

[a]In this case, a much higher amplitude noise was allowed. All values are in ns, and recovered data are shown as mean ± std.

Indeed, in the situation where noise is applied to the harmonics (rather than the lifetimes), there is a large effect on the performance of the algorithm and the recovery is much less satisfactory (large std), as shown in Table 2. In all tables, G-noise refers to Gaussian noise, specifically to the standard deviation of the Gaussian distribution from which noise was sampled.

https://dx.doi.org/10.1021/acs.jpcb.0c06946
J. Phys. Chem. B 2020, 124, 10126–10137

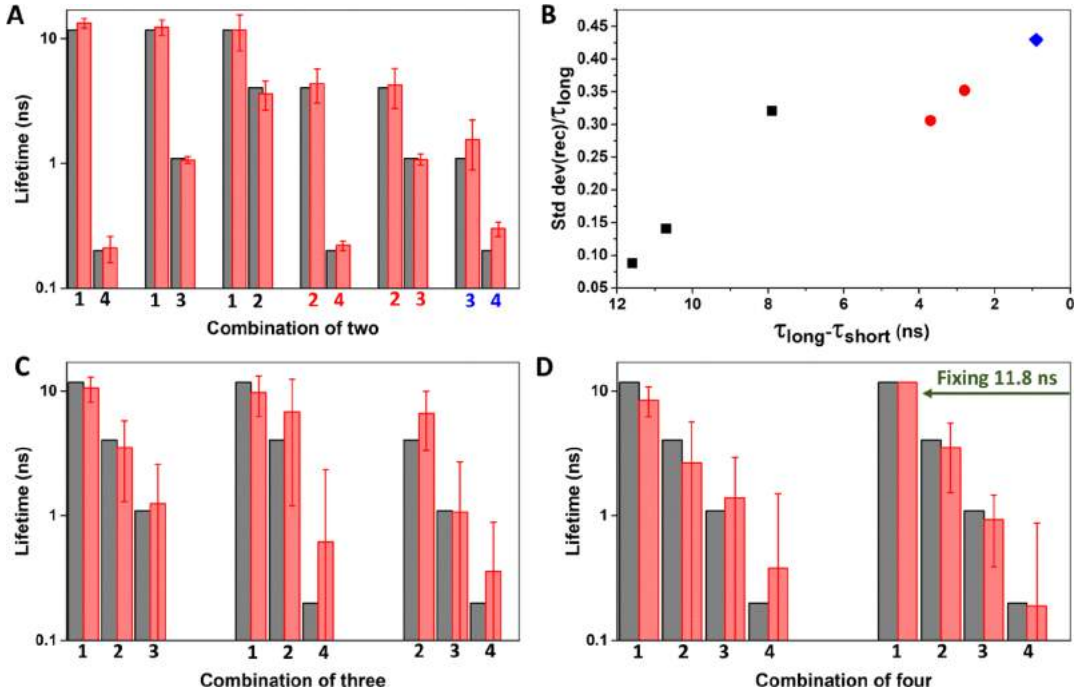

Figure 6. Results of measurements with prepared dye solutions. The expected (gray) and the recovered (red) components are shown next to each other in each case. (A) Recovery in the preparations containing two mixed dyes. (C) Recovery in the combinations of three mixed dyes. (D) Recovery in the preparation with four mixed dyes. In each case, the component id numbers correspond respectively to 1—dansyl acid, 2—fluorescein, 3—eosin Y, and 4—sulfo-Cy3. The errors in the red bars are the pixel-wise standard deviation of the recovered data. (B) For each pair combination, the difference in lifetime between the two components is plotted with the standard deviation in the recovery of the longest of the couple, showing a clear dependency. In each case, the decreasing difference between the long and short lifetimes increases the width of the distribution of the recovered long lifetime and the distribution width depends on the value of long lifetime. In the single combination of the four-component system (D), we repeated the experiment by fixing the long lifetime to the known value of 11.8 ns (right side of panel D) which substantially improves the recovery of the lifetime components.

In Table 2, Gaussian noise in one lifetime component has a much larger effect when we propagate the noise to the harmonics to be used to recover the unknown lifetimes than the direct simulation of the lifetimes with Gaussian noise (Table 1). This is due to the linear compensation which is intrinsic in the definition of harmonics in eqs 1 and 2, where we measure only the linear combinations of the lifetime components, but the relative fractions compensate the changes in lifetime to give the same location for the harmonics. However, if one of the components is known or the relative fraction of the components is known, the system can be reliably recovered even in the presence of the high level of Gaussian noise tested.

Experimental Blind Recovery of the Mixture of Dyes. In order to test the method with real data, we selected a set of four dyes with single exponential decay and prepared solutions of each individually, followed by mixtures of combinations of two, three, and finally all four of them. These samples of dyes in solution were imaged on our FLIM capable microscope, and the minimization algorithm was tested to recover the known individual components of the mixture. Figure 6 summarizes the results obtained when recovering components from these combined mixtures. We would like to note that the error bars in this figure represent the pixel-wise standard deviation obtained from a single image measurement, as opposed to the traditional experiment-wise standard error obtained from the means of all pixels in several measurements.

We show the results for the algorithm working for four unknown lifetimes and fractions, and the recovery of the four-component mixture is reasonably good. We emphasize in Figure 6D that if we fix one of the components, then the recovery of the other components is excellent, as shown where the 11.8 ns component was fixed. The reason for this is simple; it reduces the number of degrees of freedom in the problem. One can have different justifications to decide to fix a component. For example, one may know the presence of one particular species in the sample. In another situation, one may come to the realization that the distribution of one of the components is much narrower (usually the short lifetime) and may want to fix this one based on its higher confidence in order to gain precision in the others. This is usually the case due to the combined facts that, on the one hand, the harmonics converge toward the region of long lifetimes and, on the other hand, their distributions are more disperse, the higher the harmonic. Here comes the final justification which may be to fix the longer lifetime simply because it is the one with most dispersion.

Blind Component Analysis for Biological Samples. We tested the efficiency of our method in phasor FLIM data from live cells. We stained cell nuclei with a mixture of three nuclear dyes: acridine orange, NucBlue, and rose bengal. This case is considerably different from the previous case of the mixture of solutions because the dyes in live cells can compete for similar sites in the nucleus.[39,40] Another issue is that the dyes can present different lifetimes depending on the DNA base sequence.[41,42] For these reasons, the biological samples are not something that we can predict, and therefore, we show

https://dx.doi.org/10.1021/acs.jpcb.0c06946
J. Phys. Chem. B 2020, 124, 10126−10137

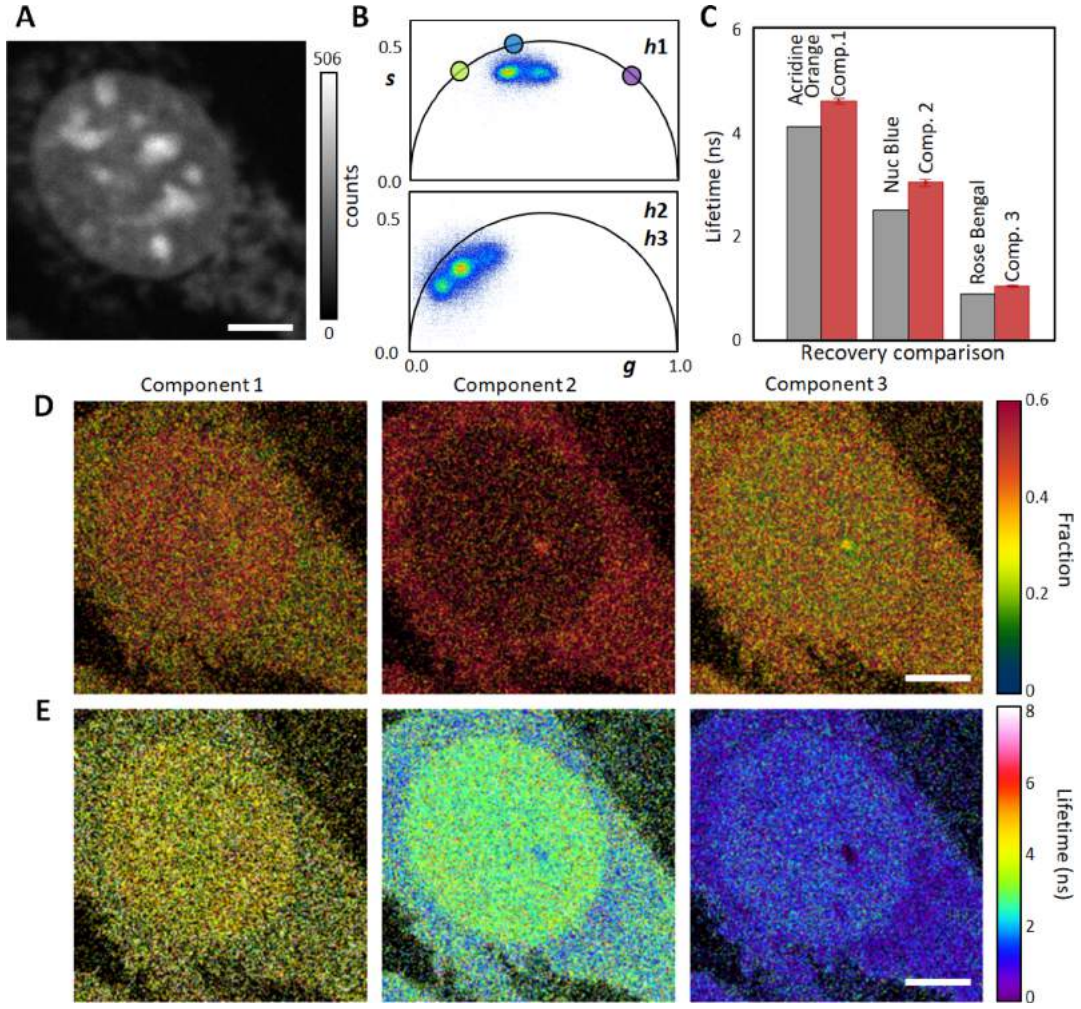

Figure 7. Three-component blind recovery in live cells. Representative FLIM experiment of a cell with the addition of nuclear dyes (acridine orange, NucBlue, and rose bengal). (A) Intensity image; the scale bar is 5 μm. In this example, we have a large number of counts in the bright dots in the nucleus (scale bar at the right of the panel). (B) Smoothed phasor plots for the first harmonic ($h1$) and the second and third harmonics together ($h2$, $h3$). The colored circles on the universal circle indicate the measured phasor position of the first harmonic of the individually measured dyes in cells; acridine orange (green), NucBlue (blue), and rose bengal (purple). (C) Bar plot comparing lifetime measurements of the individual dyes measured independently (gray) and recovered from the algorithm (red) using three blind components. Errors show the standard deviation of the recovered values in three cells. After recovering lifetimes and fractions for three components at each pixel, images are reconstructed (color-coded) with the recovered values for fractions (D) and lifetimes (E), according to the color scales on the right.

the result but we do not expect to recover the same lifetime distribution as in the samples with only one dye.

A representative FLIM experiment of the cells with the addition of the three dyes is shown in Figure 7; the intensity image is shown in Figure 7A, and the corresponding raw phasor plots (multifrequency data: $h1$, $h2$, and $h3$) are shown in Figure 7B. Additionally, we measured the lifetime of each of the dyes individually (Figure S1), to compare with the results of the blind decomposition of the mixture. The position on the phasor plot for the first harmonic of individual components from the data using only one dye at the time is indicated with colored circles (Figure 7B). The green circle is acridine orange, the blue circle is NucBlue, and the purple circle is rose bengal. The measured data do not appear on the universal semicircle, indicating that there is, in every point of the image, a linear combination of components which falls somewhere in a triangle formed by the three pure species (Figure 7B).

Inspection of the phasor plot in the first harmonic reveals two clear populations that when mapped to the original image, they correspond to the inside of the nucleus (left population) and outside of the nucleus (right population). Note that the phasors are depicted with smoothing for visualization, but the data used for the minimization were the raw unsmoothed.

We proceed to apply the minimization algorithm on the FLIM data in order to find the components and their relative fractions for a total of four cells from the same dishes (Figure 7C). These recovered values are taken only from the inside of the nucleus, meaning that they correspond to the solutions for the population in the left of the phasor plot in panel 7B. The error bars correspond to the standard deviations across the mean values obtained for the four cells, and the actual pixel variability is much larger in individual experiments, which makes sense because the distribution of species is not homogeneous across the field of view.

Remapping the recovered fractions and lifetimes to each pixel in the original image (Figure 7D,E) reveals an uneven distribution inside the nucleus and a clear difference between the inside and outside of the nucleus, corresponding to the two populations on the phasor plot.

https://dx.doi.org/10.1021/acs.jpcb.0c06946
J. Phys. Chem. B 2020, 124, 10126−10137

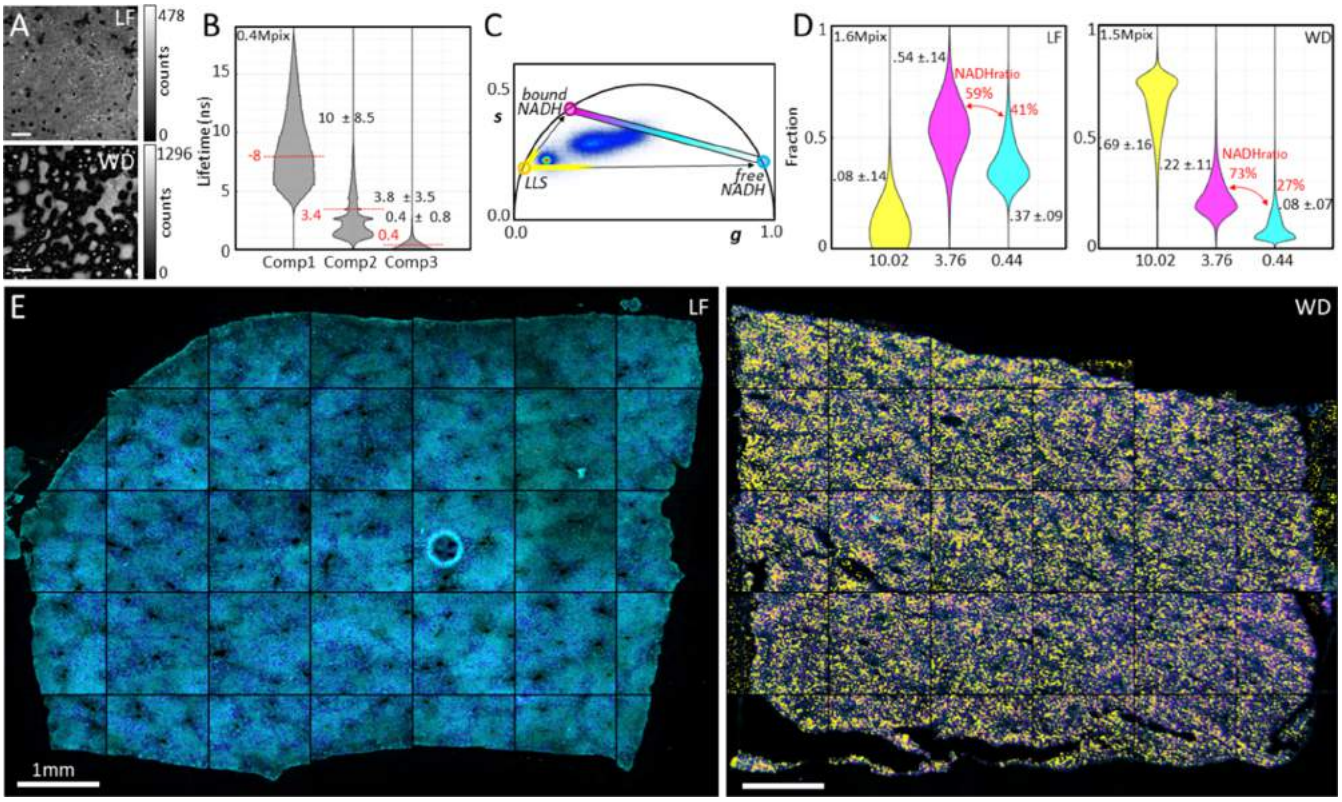

Figure 8. Three-component blind recovery in liver tissue samples allows studying metabolic changes. (A) Representative zoom-in intensity images (optical zoom = 40×) of liver slices of mice fed with LF or WD are shown (intensity scale bar at the right of the panel). The scale bar is 40 μm. High counts are observed in the fat droplets in the liver. (B) Recovered lifetimes from the algorithm using three blind components are represented as violin plots (gray) and the median ± standard deviation. Expected lifetime values for individual species reported in the literature are shown with a horizontal dotted line (red). (C) Colored circles on the universal circle indicate the recovered first harmonic phasor position of free NADH (cyan), protein-bound NADH (purple), and LLS (yellow). (D) Fractional intensity distributions of the three components in the whole tissue samples (LF and WD) imposing the recovered median lifetimes (also depicting median ± standard deviation). Bound NADH *vs* free NADH fractional intensity ratios are shown in red (by excluding LLS). (E) Color-coded phasor-FLIM images of the whole tissue sections of LF (left) and WD (right) mice models (optical zoom = 10×). The free-to-bound ratio (excluding LLS) is color coded using a magenta to cyan colormap with a yellow overlay for LLS above 75%. The scale bar is 1 mm. The bright circle in the LF sample (row 3 and column 5) is due to an air bubble.

The measured lifetimes of the separate samples each with one dye were 4.1 ns, 2.5 ns, and 0.9 ns for acridine orange, NucBlue, and rose bengal, respectively, and match with the values in the literature.[43−46] The median recovered lifetimes with our blind component analysis in the sample with all three dyes together were [4.59 ± 0.06, 3.03 ± 0.07, and 1.05 ± 0.02] with the respective intensity fractions [0.37, 0.26, and 0.36]. As mentioned before, the distribution of recovered lifetimes across all pixels in an image is much wider and, above all, not symmetric. It is noticeable that the method works under conditions of relatively low photons per pixel, although the brightest spots in the image have 500 counts; the bulk of the pixels have around 100 counts.

As an additional experiment, we imaged samples that had been used in a previous study,[35] composed of mice liver slices taken from mice being fed with two diets with completely different fat contents, one with high fat content, namely, WD, and one with LF content (see Methods section for details). The previous study reported the presence of a long-lifetime species (LLS) in the autofluorescence that was more abundant in the WD specimen in comparison to LF.[35,47] Our expectation was to blindly identify the three components in the samples: free NADH, bound NADH, and the LLS. The reported values for these components are 0.4 ns for free NADH, 3.4 ns for bound NADH,[14] and 7.8 ns for the LLS.[15]

Figure 8 shows the representative FLIM images from the liver samples. Intensity images of LF and WD in a zoomed-in version are shown in Figure 8A. The blind component algorithm was performed on a total of 10 measurements, consisting of five each of the LF and WD samples. It is important to note that even though high counts are observed in the WD sample coming from the accumulated fat, the algorithm operated with a low average of total counts. The three recovered lifetime distributions obtained from all the pixels from the LF and WD together are displayed in the violin plots of Figure 8B with their expected values.[3,14,15] The distributions are very wide, especially for the second component, and they present several peaks. This is attributed to the heterogeneity of the sample, pixels containing different proportions of the components, and makes the task of the algorithm difficult. For example, pixels in which no LLS are present can force the algorithm to find a third inexistent component. Nevertheless, the median values obtained [10.0, 3.8, and 0.4] ns for the three distributions are close to the expected lifetime values [7.8, 3.4, and 0.4] ns. These recovered values are displayed as colored circles on the universal circle on the phasor plot in Figure 8C together with the phasor transforms of all the pixels used for the blind recovery.

We then used these three recovered lifetime values to calculate the fractional intensity contribution of each of the

https://dx.doi.org/10.1021/acs.jpcb.0c06946
J. Phys. Chem. B 2020, 124, 10126−10137

three components in every pixel of LF and WD liver slices. The recovered fraction distributions for LF (left) and WD (right) are shown in Figure 8D. LLS are 8.6 times more abundant in the WD liver than in the LF, in concordance with what was previously reported.[47] In each case, we can use the three recovered fractions to express a free/bound photon intensity ratio excluding the LLS as the ratio of free or bound over the sum of the two fractions (excluding the fraction for LLS). In other words, at each pixel, we can renormalize the recovered fractions of the two shorter lifetime components to their sum, therefore obtaining the intrinsic ratios of free/bound NADH excluding the presence of the LLS. The medians of these intrinsic ratios are shown in red in Figure 8D. The obtained free NADH ratio is 41% for LF and 27% for WD, meaning that there is more bound NADH in the WD liver than in the LF. Finally, we used the three components to color-code the images (Figure 8E) and assign a colormap (magenta to cyan colorbar on the phasor plot, Figure 8C) for the ratio between the free and bound NADH lifetimes, that is, color coding the metabolic index, on which we overlay the presence of the LLS with a semitransparent yellow layer for the LLS fraction above 75%.

DISCUSSION AND CONCLUSIONS

This paper describes a general algorithm for determining the lifetime components and their weights in every pixel of a FLIM image. We describe a graphical approach for two and three components and then a general method for the recovery of four components based on a computational nonlinear minimization algorithm. While solving the set of nonlinear equations to find the lifetimes and fractions in each pixel of an image, we realized that these graphical algorithms, when implemented in MATLAB or Python, work well but the time to process an entire image can be rather slow. For an image of 256 × 256 pixels, it takes in the order of a couple of minutes for three components. A caveat of the minimization method is that the result and its speed depend on the initial assumptions (initial and boundary conditions).

The graphical method for two components is much faster (about 2 s for the entire image). We note that the graphical algorithm becomes slower when we use it for three of four components because of its nonscalability as opposed to the generalized minimization approach.

We then describe the general minimization algorithm for blind recovery of lifetimes and fractions and perform simulations in order to test it. The simulations show the efficacy of the problem when submitted to extreme situations of independent noise applied to each harmonic of the data. The algorithm also performs remarkably well in the case of real measurements of prepared mixtures of dyes in solution.

Finally, the applicability of the algorithm in biological data is shown in an example of labeling of the nucleus of a cell with three nuclear dyes. Here, the efficacy of the recovery is much harder to prove because of the variability of the probes in real live samples as they compete for binding sites in the DNA, mutual exclusion interactions, and the presence of many naturally occurring autofluorescence sources in the cells. Nevertheless, our algorithm provided results that are consistent with the expected known values in all experiments we carried out. The blind component analysis was used in mice liver sections from different diets to understand its effectiveness. The data suggest that the median of the recovered lifetime matches well with the published results, and this median value can then be used to obtain quantitative information from phasor-FLIM images, including quantification of LLS, a signature of reductive oxidation that is present in fat droplets. Furthermore, this new analysis allows for quantification of changes in metabolism even in samples where the bright species (LLS here) modifies the phasor plot to a great extent.

The blind analysis for two and three components is simple and reliable. For a larger number of components, we need to have some independent information for at least one of the components to become accurate. The phasor-based graphical algorithm works well for two and three components, and this is an achievement in the FLIM field where relatively few photons are available at each pixel of an image and even the blind resolution of two components is problematic. We could potentially use additional information such as the spectrum of the components or other spectroscopic characterization to enhance the identification of the components.

Examples of application of the proposed method could be for the analysis of clinical samples in which we do not know the composition or the relative abundance of molecular species. A blind solution pixel by pixel will allow a number of different molecular species to be detected and quantified. An example could be in describing the composition of tumor tissues in which we seek to know the abundance and location of molecules in the tumor cells. Another example is in the genomics and proteomics field wherein the existence, number, and location of molecules can be connected to the underlying biological processes.

ASSOCIATED CONTENT

Supporting Information

The Supporting Information is available free of charge at https://pubs.acs.org/doi/10.1021/acs.jpcb.0c06946.

Mathematical formalism, example application and workflow of the methodology for blind recovery of lifetime components using the phasor plot (PDF)

AUTHOR INFORMATION

Corresponding Authors

Suman Ranjit − *Department of Biochemistry and Molecular & Cellular Biology, Georgetown University, Washington, D.C., United States*; Email: suman.ranjit@georgetown.edu

Enrico Gratton − *Laboratory for Fluorescence Dynamics, Department of Biomedical Engineering, University of California, Irvine, California, United States*; orcid.org/0000-0002-6450-7391; Email: egratton22@gmail.com

Authors

Alexander Vallmitjana − *Laboratory for Fluorescence Dynamics, Department of Biomedical Engineering, University of California, Irvine, California, United States*

Belén Torrado − *Laboratory for Fluorescence Dynamics, Department of Biomedical Engineering, University of California, Irvine, California, United States*

Alexander Dvornikov − *Laboratory for Fluorescence Dynamics, Department of Biomedical Engineering, University of California, Irvine, California, United States*

Complete contact information is available at: https://pubs.acs.org/10.1021/acs.jpcb.0c06946

Author Contributions

§A.V. and B.T. contributed equally.

https://dx.doi.org/10.1021/acs.jpcb.0c06946
J. Phys. Chem. B 2020, 124, 10126−10137

Notes

The authors declare the following competing financial interest(s): E.G. has a U.S. patent for the original FLIMbox. The patent owner is the University of Illinois and E.G. has no financial interest with any company.

■ ACKNOWLEDGMENTS

We thank Dr. Moshe Levi and his lab members Dr. Xiaoxin X. Wang and Dr. Komuraiah Myakala (Department of Biochemistry and Molecular & Cellular Biology at Georgetown University) for kindly providing us the liver samples. This study was funded by National Institutes of Health (NIH) P50 GM076516 and NIH P41GM103540 to E.G. (both National Institute of General Medical Sciences).

■ ACRONYMS

FLIM	fluorescence lifetime imaging microscopy
NADH	nicotinamide adenine dinucleotide (reduced)
DIVER	deep imaging *via* emission recovery
FPGA	field programmable gate array

■ REFERENCES

(1) Digman, M. A.; Caiolfa, V. R.; Zamai, M.; Gratton, E. The Phasor Approach to Fluorescence Lifetime Imaging Analysis. *Biophys. J.* **2008**, *94*, L14−L16.

(2) Niesner, R.; Peker, B.; Schlüsche, P.; Gericke, K.-H. Noniterative Biexponential Fluorescence Lifetime Imaging in the Investigation of Cellular Metabolism by Means of NAD(P)H Autofluorescence. *Chemphyschem* **2004**, *5*, 1141−1149.

(3) Ranjit, S.; Malacrida, L.; Jameson, D. M.; Gratton, E. Fit-free analysis of fluorescence lifetime imaging data using the phasor approach. *Nat. Protoc.* **2018**, *13*, 1979−2004.

(4) Clayton, A. H. A.; Hanley, Q. S.; Verveer, P. J. Graphical representation and multicomponent analysis of single-frequency fluorescence lifetime imaging microscopy data. *J. Microsc.* **2004**, *213*, 1−5.

(5) Jameson, D. M.; Gratton, E.; Hall, R. D. The Measurement and Analysis of Heterogeneous Emissions by Multifrequency Phase and Modulation Fluorometry. *Appl. Spectrosc. Rev.* **1984**, *20*, 55−106.

(6) Redford, G. I.; Clegg, R. M. Polar Plot Representation for Frequency-Domain Analysis of Fluorescence Lifetimes. *J. Fluoresc.* **2005**, *15*, 805.

(7) Štefl, M.; James, N. G.; Ross, J. A.; Jameson, D. M. Applications of phasors to in vitro time-resolved fluorescence measurements. *Anal. Biochem.* **2011**, *410*, 62−69.

(8) Talbot, C. B.; Lagarto, J.; Warren, S.; Neil, M. A. A.; French, P. M. W.; Dunsby, C. Correction Approach for Delta Function Convolution Model Fitting of Fluorescence Decay Data in the Case of a Monoexponential Reference Fluorophore. *J. Fluoresc.* **2015**, *25*, 1169−1182.

(9) Weber, G. Resolution of the fluorescence lifetimes in a heterogeneous system by phase and modulation measurements. *J. Phys. Chem.* **1981**, *85*, 949−953.

(10) Stringari, C.; Cinquin, A.; Cinquin, O.; Digman, M. A.; Donovan, P. J.; Gratton, E. Phasor approach to fluorescence lifetime microscopy distinguishes different metabolic states of germ cells in a live tissue. *Proc. Natl. Acad. Sci. U.S.A.* **2011**, *108*, 13582−13587.

(11) Vishwasrao, H. D.; Heikal, A. A.; Kasischke, K. A.; Webb, W. W. Conformational dependence of intracellular NADH on metabolic state revealed by associated fluorescence anisotropy. *J. Biol. Chem.* **2005**, *280*, 25119−25126.

(12) Melissa, C. S.; Kristin, M. R.; Damian, K. B.; Annette, G.-F.; Jens, E.; Kevin, W. E.; Patricia, J. K.; Nirmala, R. In vivo multiphoton fluorescence lifetime imaging of protein-bound and free nicotinamide adenine dinucleotide in normal and precancerous epithelia. *J. Biomed. Optic.* **2007**, *12*, 024014.

(13) Digman, M.; Gratton, E. The phasor approach to fluorescence lifetime imaging: Exploiting phasor linear properties. *Fluorescence Lifetime Spectroscopy and Imaging*; CRC Press: Boca Raton, FL, 2014; pp 235−248.

(14) Ranjit, S.; Malacrida, L.; Stakic, M.; Gratton, E. Determination of the metabolic index using the fluorescence lifetime of free and bound nicotinamide adenine dinucleotide using the phasor approach. *J. Biophot.* **2019**, *12*, No. e201900156.

(15) Datta, R.; Alfonso-García, A.; Cinco, R.; Gratton, E. Fluorescence lifetime imaging of endogenous biomarker of oxidative stress. *Sci. Rep.* **2015**, *5*, 9848.

(16) Aguilar-Arnal, L.; Ranjit, S.; Stringari, C.; Orozco-Solis, R.; Gratton, E.; Sassone-Corsi, P. Spatial dynamics of SIRT1 and the subnuclear distribution of NADH species. *Proc. Natl. Acad. Sci. U.S.A.* **2016**, *113*, 12715.

(17) Ranjit, S.; Datta, R.; Dvornikov, A.; Gratton, E. Multicomponent Analysis of Phasor Plot in a Single Pixel to Calculate Changes of Metabolic Trajectory in Biological Systems. *J. Phys. Chem. A* **2019**, *123*, 9865−9873.

(18) Vallmitjana, A.; Dvornikov, A.; Torrado, B.; Jameson, D. M.; Ranjit, S.; Gratton, E. Resolution of 4 components in the same pixel in FLIM images using the phasor approach. *Methods Appl. Fluoresc.* **2020**, *8*, 035001.

(19) Knutson, J. R.; Beechem, J. M.; Brand, L. Simultaneous analysis of multiple fluorescence decay curves: A global approach. *Chem. Phys. Lett.* **1983**, *102*, 501−507.

(20) Verveer, P. J.; Squire, A.; Bastiaens, P. I. H. Global Analysis of Fluorescence Lifetime Imaging Microscopy Data. *Biophys. J.* **2000**, *78*, 2127−2137.

(21) Beechem, J.; Gratton, E.; Ameloot, M.; Knutson, J.; Brand, L. The Global Analysis of Fluorescence Intensity and Anisotropy Decay Data: Second-Generation Theory and Programs. *Topics in Fluorescence Spectroscopy*; Springer, 2006; pp 241−305.

(22) Nur Aida Abdul, R.; Roger, D. K.; Peter, T. C. S.; Serge, B. P.; Nur Aida Abdul, R.; Roger, D. K.; Peter, T. C. S.; Serge, B. P. Methodological considerations for global analysis of cellular FLIM/FRET measurements. *J. Biomed. Optic.* **2012**, *17*, 026013.

(23) Valm, A. M.; Cohen, S.; Legant, W. R.; Melunis, J.; Hershberg, U.; Wait, E.; Cohen, A. R.; Davidson, M. W.; Betzig, E.; Lippincott-Schwartz, J. Applying systems-level spectral imaging and analysis to reveal the organelle interactome. *Nature* **2017**, *546*, 162−167.

(24) Vu, T. Q.; Lam, W. Y.; Hatch, E. W.; Lidke, D. S. Quantum dots for quantitative imaging: from single molecules to tissue. *Cell Tissue Res.* **2015**, *360*, 71−86.

(25) Gratton, E. Measurements of Fluorescence Decay Time by the Frequency Domain Method. In *Perspectives on Fluorescence: A Tribute to Gregorio Weber*; Jameson, D. M., Ed.; Springer International Publishing: Cham, 2016; pp 67−80.

(26) Ranjit, S.; Malacrida, L.; Gratton, E. Differences between FLIM phasor analyses for data collected with the Becker and Hickl SPC830 card and with the FLIMbox card. *Microsc. Res. Tech.* **2018**, *81*, 980−989.

(27) Crosignani, V.; Jahid, S.; Dvornikov, A. S.; Gratton, E. A deep tissue fluorescence imaging system with enhanced SHG detection capabilities. *Microsc. Res. Tech.* **2014**, *77*, 368−373.

(28) Dvornikov, A.; Malacrida, L.; Gratton, E. The DIVER Microscope for Imaging in Scattering Media. *Methods Protoc.* **2019**, *2*, 53.

(29) Colyer, R. A.; Lee, C.; Gratton, E. A novel fluorescence lifetime imaging system that optimizes photon efficiency. *Microsc. Res. Tech.* **2008**, *71*, 201−213.

(30) Sanborn, M. E.; Connolly, B. K.; Gurunathan, K.; Levitus, M. Fluorescence Properties and Photophysics of the Sulfoindocyanine Cy3 Linked Covalently to DNA. *J. Phys. Chem. B* **2007**, *111*, 11064−11074.

(31) Enoki, M.; Katoh, R. Estimation of quantum yields of weak fluorescence from eosin Y dimers formed in aqueous solutions. *Photochem. Photobiol. Sci.* **2018**, *17*, 793−799.

https://dx.doi.org/10.1021/acs.jpcb.0c06946
J. Phys. Chem. B 2020, 124, 10126−10137

(32) Fleming, G. R.; Knight, A. W. E.; Morris, J. M.; Morrison, R. J. S.; Robinson, G. W. Picosecond fluorescence studies of xanthene dyes. *J. Am. Chem. Soc.* **1977**, *99*, 4306−4311.
(33) Gaviola, E. Die Abklingungszeiten der Fluoreszenz von Farbstofflösungen. *Z. Phys.* **1926**, *35*, 748−756.
(34) van de Ven, A. L.; Adler-Storthz, K.; Richards-Kortum, R. Delivery of optical contrast agents using Triton-X100, part 1: reversible permeabilization of live cells for intracellular labeling. *J. Biomed. Optic.* **2009**, *14*, 021012.
(35) Takahashi, S.; Luo, Y.; Ranjit, S.; Xie, C.; Libby, A. E.; Orlicky, D. J.; Dvornikov, A.; Wang, X. X.; Myakala, K.; Jones, B. A.; Bhasin, K.; Wang, D.; McManaman, J. L.; Krausz, K. W.; Gratton, E.; Ir, D.; Robertson, C. E.; Frank, D. N.; Gonzalez, F. J.; Levi, M. Bile Acid Sequestration Reverses Liver Injury and Prevents Progression of NASH in Western Diet-Fed Mice. *J Biol Chem* **2020**, *295*, 4733.
(36) Gill, P. E.; Wong, E. Sequential Quadratic Programming Methods. In *Mixed Integer Nonlinear Programming*; Lee, J., Leyffer, S., Eds.; Springer New York: New York, NY, 2012; pp 147−224.
(37) Marquardt, D. W. An Algorithm for Least-Squares Estimation of Nonlinear Parameters. *J. Soc. Ind. Appl. Math.* **1963**, *11*, 431−441.
(38) Nelder, J. A.; Mead, R. A Simplex Method for Function Minimization. *Comput. J.* **1965**, *7*, 308−313.
(39) Latt, S. A.; Sahar, E.; Eisenhard, M. E.; Juergens, L. A. Interactions between pairs of DNA-binding dyes: Results and implications for chromosome analysis. *Cytometry* **1980**, *1*, 2−12.
(40) Sahar, E.; Latt, S. A. Energy transfer and binding competition between dyes used to enhance staining differentiation in metaphase chromosomes. *Chromosoma* **1980**, *79*, 1−28.
(41) Harvey, B. J.; Perez, C.; Levitus, M. DNA sequence-dependent enhancement of Cy3 fluorescence. *Photochem. Photobiol. Sci.* **2009**, *8*, 1105−1110.
(42) Barcellona, M. L.; Cardiel, G.; Gratton, E. Time-resolved fluorescence of DAPI in solution and bound to polydeoxynucleotides. *Biochem. Biophys. Res. Commun.* **1990**, *170*, 270−280.
(43) Kubota, Y.; Steiner, R. F. Fluorescence decay and quantum yield characteristics of acridine orange and proflavine bound to DNA. *Biophys. Chem.* **1977**, *6*, 279−289.
(44) Lakowicz, J. R.; Laczko, G.; Gryczynski, I. 2-GHz frequency-domain fluorometer. *Rev. Sci. Instrum.* **1986**, *57*, 2499−2506.
(45) Okkelman, I. A.; Dmitriev, R. I.; Foley, T.; Papkovsky, D. B. Use of Fluorescence Lifetime Imaging Microscopy (FLIM) as a Timer of Cell Cycle S Phase. *PLoS One* **2016**, *11*, No. e0167385.
(46) Shumilov, D.; Popov, A.; Fudala, R.; Akopova, I.; Gryczynski, I.; Borejdo, J.; Gryczynski, Z.; Grygorczyk, R. Real-time imaging of exocytotic mucin release and swelling in Calu-3 cells using acridine orange. *Methods* **2014**, *66*, 312−324.
(47) Ranjit, S.; Dvornikov, A.; Dobrinskikh, E.; Wang, X.; Luo, Y.; Levi, M.; Gratton, E. Measuring the effect of a Western diet on liver tissue architecture by FLIM autofluorescence and harmonic generation microscopy. *Biomed. Opt. Express* **2017**, *8*, 3143−3154.

https://dx.doi.org/10.1021/acs.jpcb.0c06946
J. Phys. Chem. B 2020, 124, 10126−10137